Table 2. Tumorigenic Capacity of Unsorted, EpCAM$^+$, EpCAM$^-$, CD90$^+$, and CD90$^-$ Cells From Primary HCCs and Xenografts

Sample	CD133 (%)	CD90 (%)	EpCAM (%)	Cell Surface Marker	Number of Cells	Tumor Formation 2M	Tumor Formation 3M
P1	0	3.1	0	Unsorted	1×10^7	0/5	0/5
				CD90$^+$	1×10^5	0/5	0/5
				CD90$^-$	1×10^5	0/5	0/5
P2	0.06	7.0	0.06	Unsorted	1×10^7	0/5	0/5
				CD90$^+$	1×10^5	0/5	0/5
				CD90$^-$	1×10^5	0/5	0/5
P3	0	1.3	0	Unsorted	1×10^6	0/2	0/2
				CD90$^+$	1×10^4	0/4	0/4
				CD90$^-$	1×10^4	0/4	0/4
P4	0	0.6	17.5	Unsorted	1×10^6	3/4	4/4
				EpCAM$^-$	1×10^3	0/3	2/3
					1×10^4	3/4	4/4
					1×10^5	3/3	3/3
				CD90$^+$	1×10^3	0/3	0/3
					1×10^4	0/4	0/4
					1×10^5	0/3	0/3
				EpCAM$^-$ CD90$^-$	1×10^3	0/3	0/3
					1×10^4	0/4	0/4
					1×10^5	0/3	0/3
P5	0	0.8	29.7	Unsorted	1×10^6	0/5	0/5
				EpCAM$^+$	1×10^5	0/5	0/5
				CD90$^+$	1×10^5	0/5	0/5
				EpCAM$^-$ CD90$^-$	1×10^5	0/5	0/5
P6	0	0.7	0	Unsorted	1×10^6	0/2	0/2
				CD90$^+$	1×10^4	0/4	0/4
				CD90$^-$	1×10^4	0/4	0/4
P7	1.38	4.5	4.4	Unsorted	1×10^6	2/2	2/2
				EpCAM$^+$	2×10^2	0/3	0/3
					1×10^3	0/3	1/3
					1×10^4	2/4	4/4
				CD90$^+$	2×10^2	0/3	0/3
					1×10^3	0/3	0/3
					1×10^4	0/4	0/4
				EpCAM$^-$ CD90$^-$	1×10^3	0/3	0/3
					1×10^4	0/3	0/3
					1×10^5	0/4	0/4
P8	0	0.08	0	Unsorted	1×10^5	0/4	0/4
				CD90$^+$	1×10^3	0/3	0/3
				CD90$^-$	1×10^5	0/3	0/3
P9	0	0.26	0	Unsorted	1×10^5	0/4	0/4
				CD90$^+$	1×10^3	0/3	0/3
				CD90$^-$	1×10^5	0/3	0/3
P10	0	0.78	0	Unsorted	1×10^4	0/4	0/4
				CD90$^+$	1×10^3	0/3	0/3
				CD90$^-$	1×10^4	0/3	0/3
P11	0	0.1	1.54	Unsorted	5×10^4	0/2	0/2
				EpCAM$^+$	1×10^3	0/3	0/3
				CD90$^+$	1×10^3	0/3	0/3
				EpCAM$^-$ CD90$^-$	1×10^4	0/3	0/3
P12	0.06	0.05	0.09	Unsorted	1×10^5	0/3	3/3
				CD90$^+$	1×10^3	0/4	1/4
				CD90$^-$	1×10^3	0/4	1/4
					1×10^4	0/3	3/3
P13	0	0.03	67.7	EpCAM$^+$	5×10^5	4/4	NA
					5×10^4	3/3	NA
					5×10^3	3/3	NA
				EpCAM$^-$	5×10^5	0/4	NA
					5×10^4	0/3	NA
					5×10^3	0/3	NA
P14	24.0	0.06	3.1	EpCAM$^+$	5×10^3	4/5	NA
				EpCAM$^-$	5×10^3	2/5	NA
P15	0	2.45	0	CD90$^-$	5×10^4	3/4	NA
					5×10^3	1/3	NA
					5×10^2	1/3	NA
				CD90$^-$	5×10^4	2/4	NA
					5×10^3	1/3	NA
					5×10^2	0/3	NA

NA, not available.

contained definite CD133$^+$ cells (20%) (Table 2). CD90$^+$ cells were detected at variable frequencies in all 15 HCCs analyzed.

To explore the status of these CSC marker-positive cells in HCC in a large cohort, we utilized oligo-DNA microarray data from 238 HCC cases (GEO accession no.: GSE5975) to evaluate the expression of *EPCAM* (encoding EpCAM and CD326), *THY1* (encoding CD90), and *PROM1* (encoding CD133) in whole HCC tissues and nontumor (NT) tissues. Because previous studies demonstrated that CD133$^+$ and CD90$^+$ cells were detected at low frequency (~13.6% by CD133 staining and ~6.2% by CD90 staining) in HCC, but were almost nonexistent in NT liver (4, 5),[4,5] we utilized tumor/nontumor (T/N) gene-expression ratios to detect the existence of marker-positive CSCs in tumor. Accordingly, we showed that a 2-fold cutoff of T/N ratios of *EPCAM* successfully stratifies HCC samples with EpCAM$^+$ liver CSCs.[9,10]

A total of 95 (39.9%), 110 (46.2%), and 31 (13.0%) of the 238 HCC cases were thus regarded as EpCAM$^+$, CD90$^+$, and CD133$^+$ HCCs (T/N ratios: $\geq$2.0), respectively. As observed in the FACS data described above, we detected coexpression of EpCAM and CD90 in 45 HCCs (18.9%), EpCAM and CD133 in five HCCs (2%), CD90 and CD133 in five HCCs (2%), and EpCAM, CD90, and CD133 in 11 HCCs (4.6%). To clarify the characteristics of gene-expression signatures specific to stem cell marker expression status, we selected 172 HCC cases expressing a single CSC marker (34 EpCAM$^+$ CD90$^-$ CD133$^-$, 49 EpCAM$^-$ CD90$^+$ CD133$^-$, and 10 EpCAM$^-$ CD90$^-$ CD133$^+$) or all marker-negative HCCs (79 EpCAM$^-$ CD90$^-$ CD133$^-$). A class-comparison analysis with

univariate F tests and a global permutation test (×10,000) yielded a total of 1,561 differentially expressed genes. Multidimensional scaling (MDS) analysis using this gene set indicated that HCC specimens were clustered in specific groups with statistical significance ($P < 0.001$). Close examination of MDS plots revealed three major HCC subtype clusters: all marker-negative HCCs (blue spheres); EpCAM single-positive HCCs (red spheres); and CD90 single-positive HCCs (light blue spheres). $CD133^+$ HCCs (orange spheres) were rare, relatively scattered, and not clustered (Fig. 1B).

We examined the expression of representative hepatic stem/progenitor cell markers *AFP*, *KRT19*, and *DLK1* in HCCs with regard to the gene-expression status of each CSC marker (Fig. 1C). All three markers were up-regulated in $EpCAM^+$ and $CD133^+$ HCCs, compared with all marker-negative HCCs, consistent with previous findings.[10,11] However, we found no significant overexpression of *AFP*, *KRT19*, and *DLK1* in $CD90^+$ and all marker-negative HCCs.

Hierarchical cluster analyses revealed three main gene clusters that were up-regulated in $EpCAM^+$ HCCs (cluster A, 706 genes), $EpCAM^+$ or $CD133^+$ HCCs (cluster B, 530 genes), and $CD90^+$ or $CD133^+$ HCCs (cluster C, 325 genes) (Fig. 1D). Pathway analysis indicated that the enriched genes in cluster A (red bar) were associated with chromatin modification, cell-cycle regulation, and Wnt/β-catenin signaling (Fig. 1E). Genes associated with messenger RNA processing were enriched in clusters A (red bar) and B (orange bar). Surprisingly, genes in cluster C were significantly associated with pathways involved in blood-vessel morphogenesis, angiogenesis, neurogenesis, and epithelial mesenchymal transition (EMT) (light blue bar). Close examination of genes in each cluster suggested that known hepatic transcription factors (*FOXA1*), Wnt regulators (*TCF7L2* and *DKK1*), and a hepatic stem cell marker (*CD24*) were dominantly up-regulated in $EpCAM^+$ and $CD133^+$ HCCs (Fig. 1F). By contrast, genes associated with blood-vessel morphogenesis (*TIE1* and *FLT1*), EMT (*TGFB1*), and neurogenesis (*NES*) were activated dominantly in $CD90^+$ HCCs and $CD133^+$ HCCs.

$CD90^+$ HCC Cells Share Features With Mesenchymal Vascular Endothelial Cells. Because $CD133^+$ HCCs were relatively rare and constituted only 13% (microarray cohort) to 20% (FACS cohort) of all HCC samples analyzed, we focused on the characterization of EpCAM and CD90. To clarify the cell identity of $EpCAM^+$ or $CD90^+$ cells in primary HCCs, we performed IHC analysis of 18 needle-biopsy specimens of premalignant dysplastic nodules (DNs), 102 surgically resected HCCs, and corresponding NT liver tissues. When examining the expression of EpCAM and CD90 in cirrhotic liver tissue by double-color IHC analysis, we found that $EpCAM^+$ cells and $CD90^+$ cells were distinctively located and not colocalized (Supporting Fig. 1A). Immunoreactivity (IR) to anti-CD90 antibodies (Abs) was detected in vascular endothelial cells (VECs), inflammatory cells, fibroblasts, and neurons, but not in hepatocytes or cholangiocytes, in the cirrhotic liver (Supporting Fig. 1B, panels a,b). IR to anti-EpCAM Abs was detected in hepatic progenitors adjacent to the periportal area and bile duct epithelial cells in liver cirrhosis (Supporting Fig. 1B, panels c,d).

IR to anti-EpCAM Abs was detected in 37 of 102 surgically resected HCCs (Fig. 2A, panel b), but not in 18 DNs (Fig. 2A, panel a). By contrast, no tumor epithelial cells (TECs) showing IR to anti-CD90 Abs were found in any of the 18 DNs or 102 HCCs examined (Fig. 2A, panels c,d). However, we identified $CD90^+$ cells that were morphologically similar to VECs or fibroblasts within the tumor nodule in 37 of the 102 surgically resected HCC tissues (≥5% positive staining in a given area). IR to anti-CD90 Abs was also detected in hepatic mesenchymal tumors (Supporting Fig. 1C, panels a-c), indicating that CD90 is also a marker of liver stromal tumors.

Double-color IHC and immunofluorescence (IF) analysis confirmed the distinct expression of EpCAM and CD90 in HCC (Fig. 2B), consistent with the FACS data (Fig. 1A). Quantitative real-time polymerase chain reaction (qPCR) analysis of sorted $EpCAM^+$, $CD90^+$, and $EpCAM^-$ $CD90^-$ cells after $CD45^+$ cell depletion indicated that the hepatic stem/progenitor markers, *AFP* and *KRT19*, were up-regulated in $EpCAM^+$ cells (red bar), whereas the mesenchymal markers, *KIT* and *FLT1*, were up-regulated in $CD90^+$ cells (orange bar), compared with $EpCAM^-$ $CD90^-$ cells (blue bar) (Fig. 2C). The hepatocyte marker, *CYP3A4*, was down-regulated in $EpCAM^+$ cells and not detected in $CD90^+$ cells, compared with $EpCAM^-$ $CD90^-$ cells. *POU5F1* and *BMI1* were equally up-regulated in both $EpCAM^+$ and $CD90^+$ cells, compared with $EpCAM^-$ $CD90^-$ cells.

EpCAM and CD90 were independently and distinctively expressed in different cellular lineages, so we evaluated the staining of EpCAM and CD90 separately and analyzed the clinicopathological characteristics of surgically resected HCC cases. HCCs were regarded marker positive if ≥5% positive staining was detected in a given area. The existence of $EpCAM^+$

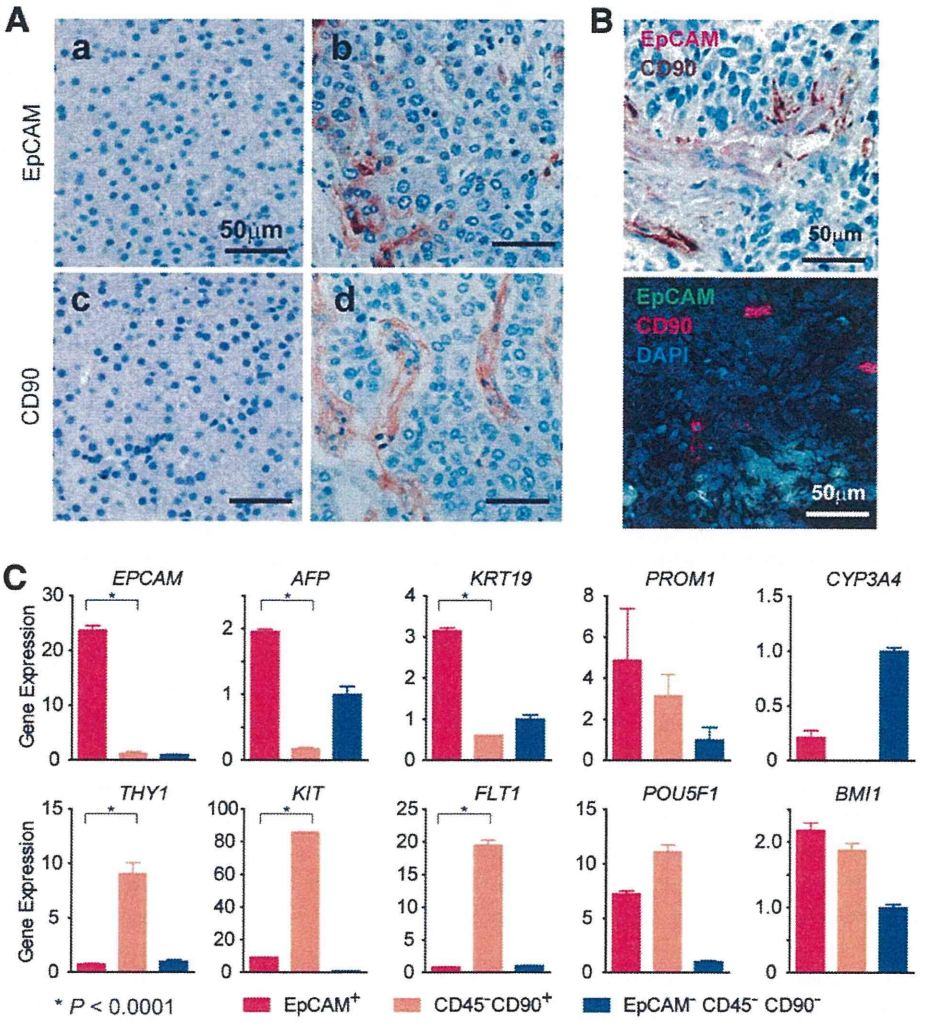

Fig. 2. Distinct EpCAM$^+$ and CD90$^+$ cell populations in HCC. (A) Representative images of EpCAM and CD90 staining in dysplastic nodule (panels a,c) and HCC (panels b,d) by IHC analysis (scale bar, 50 μm). EpCAM (panels a,b) and CD90 (panels c,d) immunostaining is depicted. (B) Upper panel: representative images of EpCAM (red) and CD90 (brown) double staining in HCC by IHC (scale bar, 50 μm). Lower panel: representative images of EpCAM (green) and CD90 (red) staining with 4'6-diamidino-phenylindole (DAPI) (blue) in HCC by IF (scale bar, 50 μm). (C) qPCR analysis of sorted EpCAM$^+$ (red bar), CD90$^+$ (orange bar), or EpCAM$^-$ CD90$^-$ (blue bar) derived from a representative primary HCC. Experiments were performed in triplicate, and data are shown as mean ± standard error of the mean.

cells (≥5%) was characterized by poorly differentiated morphology and high serum AFP values with a tendency for portal vein invasion, whereas the existence of CD90$^+$ cells (≥5%) was associated with poorly differentiated morphology and a tendency for large tumor size (Supporting Tables 2 and 3). Notably, the existence of CD90$^+$ cells was associated with a high incidence of distant organ metastasis, including lung, bone, and adrenal gland, within 2 years after surgery, whereas EpCAM$^+$ cell abundance appeared unrelated to distant organ metastasis.

We evaluated the characteristics of EpCAM$^+$ or CD90$^+$ cells in seven representative HCC cell lines. Morphologically, all EpCAM$^+$ cell lines (HuH1, HuH7, and Hep3B) showed a polygonal, epithelial cell shape, whereas three of four CD90$^+$ cell lines (HLE, HLF, and SK-Hep-1) showed a spindle cell shape (Fig. 3A). EpCAM$^+$ cells were detected in 11.5%, 57.7%, and 99.6% of sorted HuH1, HuH7, and Hep3B cells, respectively. A small CD90$^+$ cell population (0.66%) was observed in PLC/PRL/5, whereas 91.3%, 10.8%, and 59.0% of CD90$^+$ cells were detected in HLE, HLF, and SK-Hep-1, respectively. Compared with primary HCCs, only EpCAM$^+$ or CD90$^+$ cells were detected in liver cancer cell lines under normal culture conditions (Fig. 3B), suggesting that these cell lines contain a relatively pure cell population most likely obtained by clonal selection through the establishment process.

A class-comparison analysis with univariate t tests and a global permutation test (×10,000) of microarray data yielded two main gene clusters up-regulated in EpCAM$^+$ cell lines (HuH1, HuH7, and Hep3B) (cluster I, 524 genes) or in CD90$^+$ cell lines (HLE, HLF, and SK-Hep-1) (cluster II, 366 genes) (Fig. 3C). PLC/PRL/5 showed intermediate gene-expression patterns between EpCAM$^+$ and CD90$^+$ cell lines using this gene set. Pathway analysis indicated that the genes

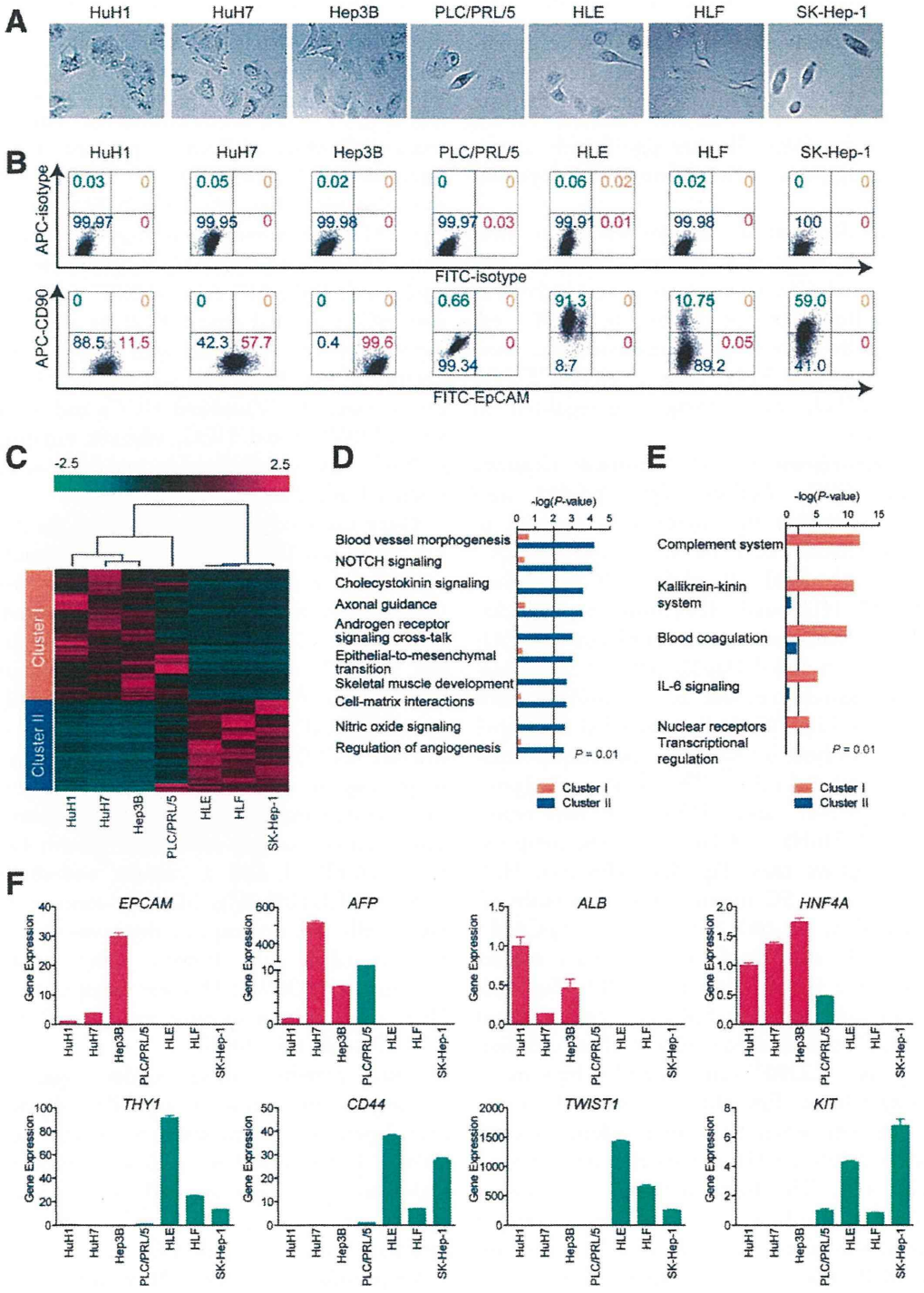

Fig. 3. Characteristics of HCC cell lines defined by EpCAM and CD90. (A) Representative photomicrographs of EpCAM$^+$CD90$^-$ and EpCAM$^-$ CD90$^+$ HCC cell lines. (B) Representative FACS data of EpCAM$^+$CD90$^-$ and EpCAM$^-$ CD90$^+$ HCC cell lines stained with fluorescein isothiocyanate (FITC)-EpCAM and APC-CD90 Abs. (C) Heat-map images of seven HCC cell lines based on 890 EpCAM/CD90-coregulated genes. Each cell in the matrix represents the expression level of a gene in an individual sample. Red and green cells depict high and low expression levels, respectively, as indicated by the scale bar. (D and E) Pathway analysis of EpCAM/CD90-coregulated genes. Canonical signaling pathways activated in cluster I (orange bar) or II (blue bar) with statistical significance ($P < 0.01$) are shown. (F) qPCR of representative differentially expressed genes identified by microarray analysis (C) in seven HCC cell lines.

enriched in cluster II were mainly associated with blood-vessel morpho- and angiogenesis (Fig. 3D). By contrast, the enriched genes in cluster I were significantly associated with known hepatocyte functions ($P < 0.01$) (Fig. 3E). In addition, we identified that the enriched genes in cluster II were significantly associated with neurogenesis, skeletal muscle development, and EMT.

We used qPCR to validate that known hepatic stem cell (HSC) and hepatocyte markers, such as *AFP, EPCAM, ALB*, and *HNF4A* genes, were up-regulated in $EpCAM^+$ cell lines, but not detected in $CD90^+$ cell lines (Fig. 3F). By contrast, genes associated with mesenchymal lineages and EMT, such as *KIT, TWIST1, CD44*, and *THY1*, were strongly up-regulated in $CD90^+$ cell lines.

Unique Tumorigenicity and Metastasis Capacity of Distinct CSCs Defined by EpCAM and CD90. We investigated the tumorigenic capacity of $EpCAM^+$ or $CD90^+$ cells by subcutaneously (SC) injecting 1×10^5 sorted cells of four HCC cell lines (HuH1, HuH7, HLE, and HLF) into nonobese diabetic, severe combined immunodeficient (NOD/SCID) mice. We excluded Hep3B cells for the evaluation of tumorigenicity because almost 100% of cells were EpCAM positive. We further excluded SK-Hep-1 cells from the analysis because they potentially originated from endothelial cells.[12] The highly tumorigenic capacities of $EpCAM^+$ and $CD90^+$ cells were reproduced in HuH1, HuH7, and HLF cell lines, compared with marker-negative cells (Fig. 4A). However, HLE cells did not produce SC tumors, even 12 months after transplantation, in NOD/SCID mice. $EpCAM^+$ cells from HuH1 and HuH7 formed larger tumors more rapidly than $CD90^+$ cells from HLF (Fig. 4B). IHC analyses indicated that $EpCAM^+$ cells did not produce $CD90^+$ cells and *vice versa* in these cell lines *in vivo* (Fig. 4C). $CD90^+$ cells showed a high metastatic capacity, whereas $EpCAM^+$ cells showed no metastasis to the lung when SC tumor volume reached approximately 2,000 (HuH1 and HuH7) or 700 mm^3 (HLF) (Fig. 4D). The high metastatic capacity of PLC/PRL/5 cells, which contain a small population of $CD90^+$ cells, was also confirmed after SC injection into NOD/SCID mice (data not shown). $CD90^+$ cells could divide to generate both $CD90^+$ and $CD90^-$ cells, and $CD90^+$ cells showed a high capacity to invade and form spheroids with overexpression of *TWIST1* and *TWIST2*, which are known to activate EMT programs in HLF cells (Supporting Fig. 2A-D).

We next evaluated the tumorigenic/metastatic capacity of $CD45^-$ tumor cells using 12 fresh primary HCC specimens (P1-P12) that had been surgically resected (Table 2). We further evaluated the tumorigenicity of EpCAM/CD90 sorted cells obtained from xenografts derived from primary HCCs (Supporting Fig. 3A). Of these, we confirmed the tumorigenicity of cancer cells obtained from six primary HCCs after SC injection into NOD/SCID mice within 3 months after transplantation (Fig. 5A; Table 2; Supporting Fig. 3B). $EpCAM^+$ cells derived from four HCCs (P4, P7, P13, and P14) showed highly tumorigenic capacities, compared with $EpCAM^-$ cells. $CD90^+$ cells derived from two HCCs showed equal (P12) or more-tumorigenic capacities (P15), compared with $CD90^-$ cells. Tumorigenicity of $EpCAM^+$ cells was observed in three hepatitis C virus (HCV)-related HCCs and an hepatitis B virus (HBV)-related HCC, whereas tumorigenicity of $CD90^+$ cells was observed in two HBV-related HCCs (Tables 1 and 2).

Using unsorted cells, we compared the frequency of $EpCAM^+$ and $CD90^+$ cells in primary and xenograft tumors and found that $EpCAM^+$ cells remained, but $CD90^+$ cells disappeared, in secondary tumors derived from P4 or P7, whereas $EpCAM^+$ cells disappeared, but $CD90^+$ cells remained, in secondary tumors derived from P12 (Fig. 5B). Morphologically, tumorigenic $EpCAM^+$ cells showed an epithelial cell shape, whereas $CD90^+$ cells showed a mesenchymal VEC shape (Fig. 5C and Supporting Fig. 3C). FACS analysis indicated that P12 HCC cells showed abundant expression of vascular endothelial growth factor receptor (VEGFR) 1 and a vascular endothelial marker endoglin (CD105) (Fig. 5D). By contrast, P4 and P7 HCC cells did not express these vascular endothelial markers (data not shown). Lung metastasis was detected in NOD/SCID mice transplanted with P12 HCC cells, but not in mice transplanted with P4 and P7 HCC cells (Fig. 5E,F).

Taken together, these results suggest that the tumorigenic and metastatic capability of primary HCC may depend on the presence of distinct $EpCAM^+$ or $CD90^+$ CSCs. $EpCAM^+$ cells were associated with a high tumorigenic capacity with hepatic epithelial stem cell features, whereas $CD90^+$ cells were related to the metastatic propensity with VEC features.

Suppression of Lung Metastasis Mediated by $CD90^+$ CSCs by Imatinib Mesylate. We previously demonstrated that Wnt/β-catenin signaling inhibitors could successfully attenuate the tumorigenic capacity of $EpCAM^+$ CSCs in HCC.[8,10] To explore the potential molecular targets activated in $CD90^+$ CSCs, we investigated the expression of the known VEC markers, CD105, VEGFR1 (encoded by *FLT1*), and

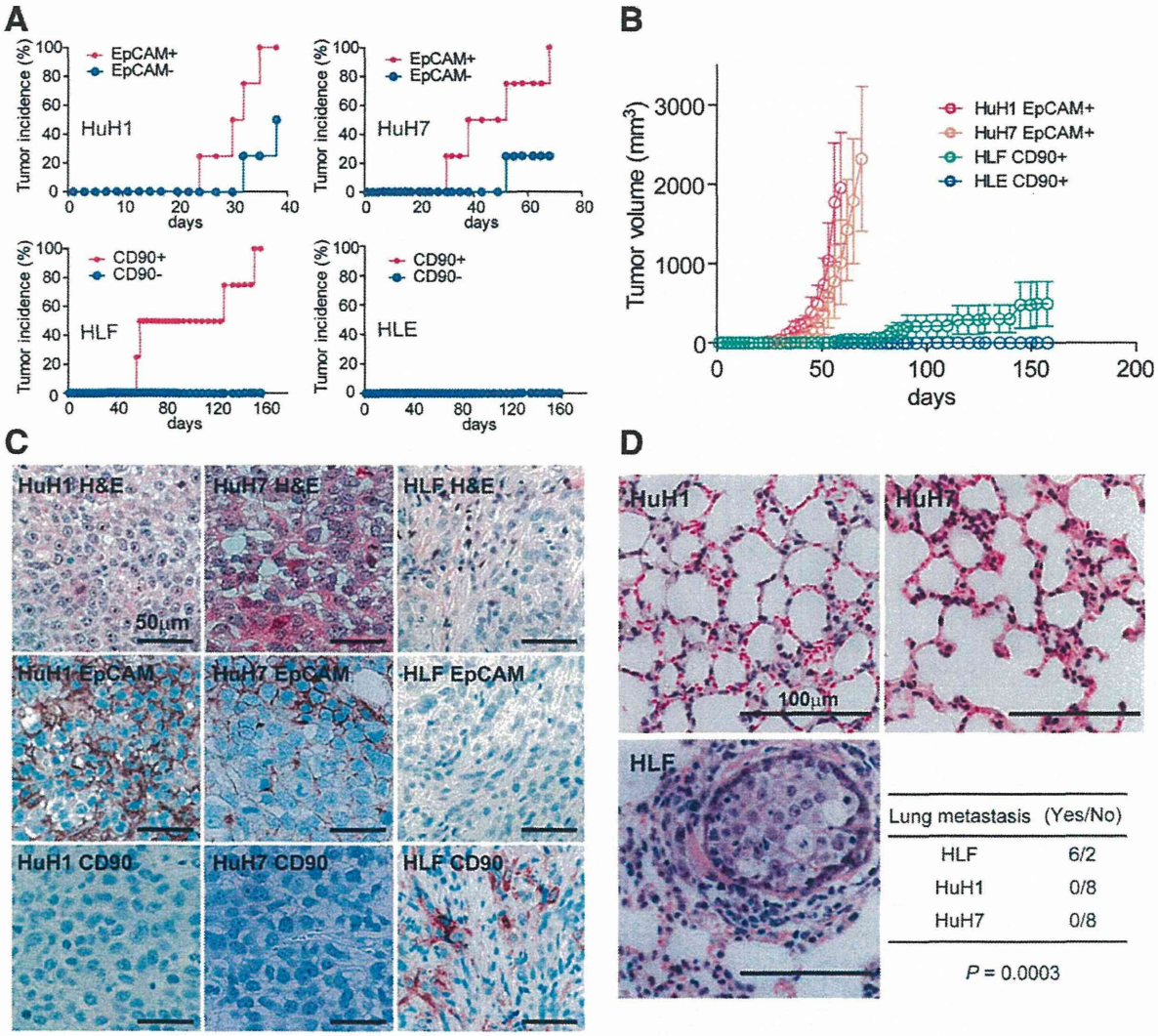

Fig. 4. Distinct tumorigenic/metastatic capacities of HCC cell lines defined by EpCAM and CD90. (A) Tumorigenicity of 1×10^5 cells sorted by anti-EpCAM (HuH1 and HuH7) or anti-CD90 (HLE and HLF) Abs. Data are generated from 8 mice/cell line. (B) Tumorigenic ability of $EpCAM^+$ and $CD90^+$ sorted cells in NOD/SCID mice. Aggressive tumor growth in the SC lesion was observed in $EpCAM^+$ HuH1 or HuH7 cells, compared with $CD90^+$ HLE or HLF cells. $EpCAM^+$ (1×10^5) or $CD90^+$ cells were injected. Tumor-volume curves are depicted as mean ± standard deviation of 4 mice/group. (C) Histological analysis of $EpCAM^+$ or $CD90^+$ cell-derived xenografts. Hematoxylin and eosin (H&E) staining of a SC tumor (upper panels) and IHC of the tumor with anti-EpCAM (middle panels) or anti-CD90 Abs (bottom panels) are shown (scale bar, 50 μm). (D) Metastasis was evaluated macroscopically and microscopically in the left and right lobes of the lung separately in each mouse (n = 4) (scale bar, 100 μm).

c-Kit (encoded by *KIT*), in cell lines and showed that they were abundantly expressed in $CD90^+$ cell lines, but not $EpCAM^+$ cell lines (Fig. 6A). No expression of VEGFR2 was detected in this set of cell lines, suggesting that molecular reagents specifically targeting VEGFR2 may have no effects on $CD90^+$ CSCs. CD44, a stem cell marker that functionally regulates redox status and is a potential target of $CD90^+$ CSCs, was also abundantly expressed in $CD90^+$ cell lines (Supporting Fig. 4A), consistent with previous data.[5,13] No significant difference was detected in the expression of the hematopoietic marker, CD34, or ABCG2 between $EpCAM^+$ and $CD90^+$ cell lines (Supporting Fig. 4A).

Among these molecular targets, we focused on the characterization of c-Kit because the c-Kit tyrosine kinase inhibitor, imatinib mesylate, is readily available, is widely used for the treatment of gastrointestinal stromal tumor with activation of c-Kit, and may have potential antitumor activity against a subset of HCC.[14] We explored the effect of imatinib mesylate on HCC cell lines and found that treatment with 10

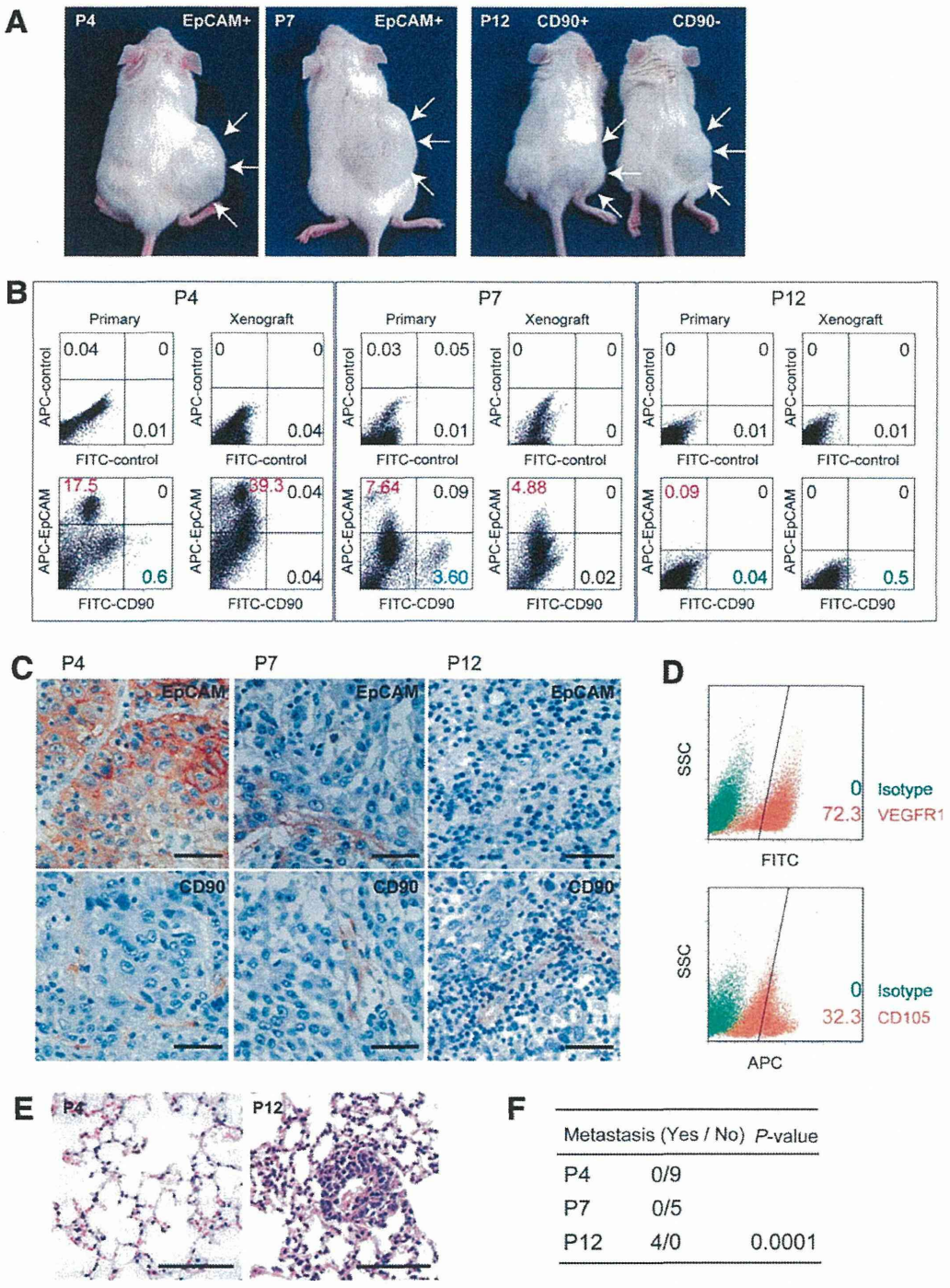

Fig. 5. Tumorigenic/metastatic capacities of EpCAM$^+$ and CD90$^+$ cells in primary HCC. (A) Representative NOD/SCID mice with SC tumors (white arrows) from EpCAM$^+$ P4 or P7 cells (left and middle panels) and CD90$^+$ or CD90$^-$ P12 cells (right panel). (B) FACS analysis of CD90 and EpCAM staining in primary HCCs and the corresponding secondary tumors developed in NOD/SCID mice. Unsorted cells (1×10^6 cells in P4 and P7 or 1×10^5 cells in P12) were SC injected to evaluate the frequency of each marker-positive cell in primary and secondary tumors. (C) IHC analysis of EpCAM and CD90 in primary HCCs P4, P7, and P12 (scale bar, 50 μm). (D) FACS analysis of VEGFR1 (Alexa488) and CD105 (APC) in primary HCC P12. (E) Hematoxylin and eosin staining of lung tissues in P4 and P12 (scale bar, 200 μm). (F) Frequency of lung metastasis in NOD/SCID mice SC transplanted using unsorted primary HCC cells.

μM reduced cell proliferation and spheroid formation in CD90$^+$ cell lines, but had no effect on EpCAM$^+$ cell lines (Supporting Fig. S4B,C).

We further explored the effect of imatinib mesylate *in vivo*. Because EpCAM$^+$ and CD90$^+$ cells reside in the primary HCC, but not in established cell lines, we SC injected HuH7 and HLF cell lines to generate tumors organized by EpCAM$^+$ and CD90$^+$ CSCs. Interestingly, when HLF cells were coinjected with HuH7 cells, EpCAM$^+$ cells could metastasize to the lung, whereas

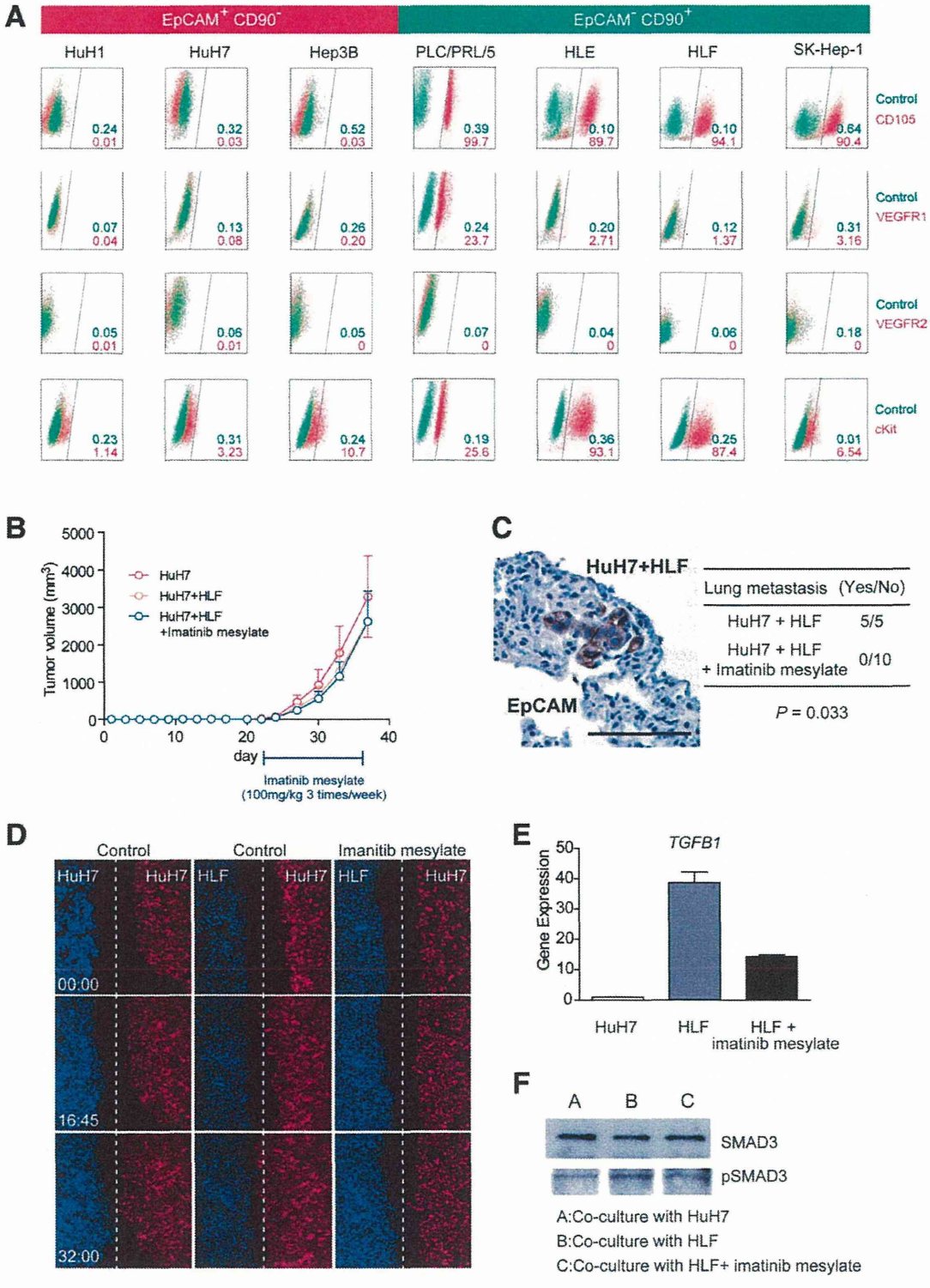

Fig. 6.

SC primary tumors showed no difference in size (Fig. 6B,C). Furthermore, although imatinib mesylate treatment had little effect on the size of primary SC tumors, it significantly suppressed lung metastasis in primary tumors (Fig. 6C). These data suggest that $CD90^+$ cells are not only metastatic to the distant organ, but also help the metastasis of $CD90^-$ cells, including $EpCAM^+$ cells, which originally have no distant metastatic capacity. Our data further suggest that imatinib mesylate can inhibit distant organ metastasis by suppressing $CD90^+$ metastatic CSCs, albeit with little effect on $EpCAM^+$ tumorigenic epithelial stem-like CSCs.

To explore the potential mechanism of how $CD90^+$ cells dictate the metastasis of $EpCAM^+$ cells, we utilized coculture systems and time-lapse image analysis. Wound-healing analysis clearly indicated that motility of HuH7 cells was enhanced when HLF cells were cocultured, and this effect was abolished by imatinib mesylate treatment (Fig. 6D; see Supporting Videos 1-3). HLF cells abundantly expressed *TGFB1*, compared with HuH7 cells, and its expression was dramatically suppressed by imatinib mesylate treatment (Fig. 6E). Mothers against decapentaplegic homolog 3 (Smad3) phosphorylation was augmented in HuH7 cells when cocultured with HLF cells, and this effect was attenuated when cocultured with HLF cells pretreated with imatinib mesylate.

Taken together, our data suggest that liver CSCs are not a single entity. Liver CSCs defined by different markers show unique features of tumorigenicity/metastasis with phenotypes closely associated with committed liver lineages. These distinct CSCs may collaborate to enhance tumorigenicity and metastasis of HCCs.

Discussion

The current investigation demonstrates that CSC marker expression status may be a key determinant of cancer phenotypes, in terms of metastatic propensity and chemosensitivity, to certain molecularly targeted therapies. EpCAM appears to be an epithelial tumorigenic CSC marker, whereas CD90 seems to be a mesenchymal metastatic CSC marker associated with expression of c-Kit and chemosensitivity to imatinib mesylate. Imatinib mesylate may be effective in inhibiting metastasis, but has little effect on primary $EpCAM^+$ HCC cell growth.

We investigated the frequency of three CSC markers (EpCAM, CD90, and CD133) in 15 primary HCCs with a confirmed cell viability of $\geq$70% and found that three HCCs contained $CD133^+$ cells, seven HCCs contained $EpCAM^+$ cells, and all HCCs contained $CD90^+$ cells. Among them, we confirmed the perpetuation of $CD133^+$ cells derived from three HCCs (P7, P12, and P14; data not shown), $EpCAM^+$ cells derived from four HCCs (P4, P7, P13, and P14), and $CD90^+$ cells derived from two HCCs (P12 and P15). Recent studies showed that at least 8 of 21 HCCs (38%)[4] and 13 of 13 HCCs (100%)[5] contained tumorigenic $CD133^+$ or $CD90^+$ CSCs, respectively. Recent IHC and tissue microarray studies also demonstrated that $CD133^+$ and $CD90^+$ cells were detected in 24.8% ($\geq$1% of tumor cells) and 32.2% ($\geq$5% of tumor cells) of HCC cases examined, respectively.[15,16]

One possible explanation of the comparatively low frequency of $CD133^+$ liver CSCs identified in our study is that we used the monoclonal Ab CD133/2, whereas Ma et al. used CD133/1. Another possible explanation is the difference of etiology related to hepatocarcinogenesis. We examined tumorigenicity using 15 HCCs (five HBV related, four HCV related, three non-B, non-C hepatitis [NBNC] related, and three alcohol related) and identified that tumorigenic CSCs were only obtained from HBV- or HCV-related cases. Previous liver CSC studies were performed using HBV-related HCCs,[4,5] and a recent study showed that

Fig. 6. Suppression of lung metastasis mediated by $CD90^+$ CSCs by imatinib mesylate. (A) FACS analysis of seven HCC cell lines stained by APC-CD105, Alexa 488/VEGFR1, APC/VEGFR2, and Alexa 488/c-Kit Abs or isotype control. (B) Tumorigenicity of 5×10^5 HuH7 cells and 2.5×10^5 HuH7 cells plus 2.5×10^5 HLF cells treated with imatinib mesylate or control phosphate-buffered saline (PBS) (200 μL/mouse) orally ingested three times per week (100 mg/kg) for 2 weeks. Data are generated from 5 mice per condition. (C) IHC analysis of EpCAM in lung metastasis detected in NOD/SCID mice SC injected with 2.5×10^5 HuH7 cells and 2.5×10^5 HLF cells. Metastasis was evaluated macro- and microscopically in the left and right lobes of the lung separately in each mouse ($n = 5$) (scale bar, 100 μm). (D) Cell motility of HuH7 cells cocultured with HuH7, HLF, or HLF cells with imatinib mesylate (10 μM) was monitored in a real-time manner by time-lapse image analysis. HuH7 and HLF cells were labeled with the lipophilic fluorescence tracer, DiI (indicated as red) or DiD (indicated as blue), and incubated in a μ-Slide eight-well chamber overnight. Silicone inserts were detached and the culture media replaced with Dulbecco's modified Eagle's medium containing 10% fetal bovine serum, including 0.1% dimethyl sulfoxide (DMSO) (control) or 10 μM of imatinib mesylate dissolved in DMSO (final concentration 0.1%). Immediately after the medium change, cells were cultured at 37°C in 5% CO_2 and time-lapse images were captured for 72 hours. (E) qPCR analysis of *TGFB1* in HuH7 (white bar), HLF (gray bar), and HLF cells pretreated with imatinib mesylate for 24 hours. (F) Smad3 and its phosphorylation evaluated by western blotting. HuH7 cells and HLF cells were harvested in cell culture inserts and treated with DMSO (0.1%) or imatinib mesylate (10 μM) for 24 hours. Cell culture inserts were washed with PBS, cocultured with HuH7 cells for 8 hours, and then removed. HuH7 cells were lysed using radioimmunoprecipitation assay buffer for western blotting. (A) HuH7 cells cocultured with HuH7 cells. (B) HuH7 cells cocultured with HLF cells. (C) HuH7 cells cocultured with HLF cells pretreated with imatinib mesylate.

HBV X may play a role in generating $EpCAM^+$ CSCs.[17] The role of hepatitis virus infection on the generation of CSCs is still unclear and should be clarified in future studies.

We were unable to confirm the tumorigenicity of $CD90^+$ cells in 13 of 15 HCCs, but we observed abundant $CD90^+$ cells in more-advanced HCCs by IHC (data not shown). Tumorigenic $CD90^+$ cells may emerge at a later stage of hepatocarcinogenesis, and the majority of $CD90^+$ cells in early HCCs may be cancer-associated VECs without tumorigenic capacity. Furthermore, we identified tumorigenic $CD90^+$ cells only from HBV-related HCCs, and a recent study suggested that expression of CD90 was associated with HBV infection.[16] We could not detect the small population of $CD90^+$ HuH7 and Hep3B cells reported on by Yang et al. However, because we identified a small population of $CD90^+$ HuH7 cells after treatment with 5-FU (manuscript in preparation), it is conceivable that different cellular stress statuses may explain the observed differences between our findings and those of Yang et al.

The majority of CSC markers discovered thus far are almost identical to those found in healthy tissue stem cells or embryonic stem cells. However, with regard to the liver, the characteristics of healthy hepatic stem/progenitor cells isolated using different stem cell markers are currently under investigation. A recent article examined the characteristics of $EpCAM^+$ and $CD90^+$ oval cells isolated from 2-acetylaminofluorene/partial hepatectomy or D-galactosamine-treated rats.[18] Interestingly, $EpCAM^+$ and $CD90^+$ oval cells represent two distinct populations: The former expresses classical oval cell markers, such as AFP, OV-1, and cytokeratin-19 (CK-19), whereas the latter expresses desmin and alpha smooth muscle actin, but not AFP, OV-1, or CK-19, which indicates that $CD90^+$ populations are more likely to be mesenchymal cells. Another study has demonstrated that mesenchymal cells can interact with HSCs to regulate cell-fate decision.[19] We found that $EpCAM^+$ and $CD90^+$ cells isolated from liver cancer are distinct in terms of gene- and protein-expression patterns in both primary liver cancers and cell lines. Furthermore, these distinct CSCs can interact to regulate the tumorigenicity and metastasis of HCC. Molecular characteristics of $EpCAM^+/CD90^+$ CSCs may potentially reflect the cellular context of healthy stem or progenitor cells.

Although our study strongly indicates that abundant $CD90^+$ cells in a tumor is a risk for distant metastasis in liver cancer, the cell identity and role of $CD90^+$ cells remains elusive. As our IHC, FACS, and xenotransplantation assays revealed, some $CD90^+$ cells in liver cancer may be cancer-associated VECs or fibroblasts that cannot perpetuate in the xenograft. Recent findings have suggested the importance of stromal cells in tumorigenesis and cancer metastasis,[20-22] so it is possible that these cells may help TECs invade and intravasate into blood vessels, thus playing crucial roles in metastasis.

Another possibility is that $CD90^+$ cells are cancer cells with features of fibroblasts (having undergone EMT) or VECs (having undergone vasculogenic mimicry; VM) that can invade, intravasate, and metastasize cells to distant organs. Recently, two groups reported that a subset of tumor VECs originate from glioblastoma CSCs.[23,24] We successfully confirmed the tumorigenicity and metastatic capacity of $CD90^+$ cells that were morphologically identical to VECs from primary HCCs that could perpetuate in the xenograft. However, a recent study demonstrated that $CD90^+$ HCC cells express glypican-3, a marker detected in hepatic epithelial cells.[25] Further studies are warranted to clarify the nature and role of $CD90^+$ HCC cells.

In our study, $CD90^+$ cells expressed the endothelial marker, c-Kit, CD105, and VEGFR1, and a mesenchymal VEC morphology and high metastatic capacity were confirmed in both primary liver cancer and cell lines. We further confirmed that $CD90^+$ liver cancer cells showed chemosensitivity to imatinib mesylate, suggesting that cancer cells committed to mesenchymal endothelial lineages could be eradicated by the compound. Although imatinib mesylate treatment had little effect on the size of primary tumors originated from both $EpCAM^+$ and $CD90^+$ CSCs, it significantly suppressed lung metastasis *in vivo*. These data are consistent with a recent phase II study demonstrating the tolerable toxicity, but limited efficacy, of imatinib mesylate alone for unresectable HCC patients. Eligibility of imatinib mesylate for advanced HCC patients may be restricted to the HCC subtypes organized by $CD90^+$ CSCs with a highly metastatic capacity and VEC features. Therefore, a combination of compounds targeting $EpCAM^+$ tumorigenic CSCs as well as $CD90^+$ metastatic CSCs may be required for the eradication of HCC and should be tested in the future.

Acknowledgments: The authors thank Ms. Nami Nishiyama and Ms. Mikiko Nakamura for their excellent technical assistance.

References

1. Tsai WL, Chung RT. Viral hepatocarcinogenesis. Oncogene 2010;29: 2309-2324.